BMC Medical Imaging

RESEARCH

Open Access

Analysis of features of papillary thyroid carcinoma on color Doppler ultrasound images: implications for lymph node metastasis

Lu Cao[1,2], Ying Cao[1,2], Xiangru Wang[1], Xinxin Lu[1], Fangxi Zhao[1], Lei Sun[1], Hua Wang[1*] and Xiaopeng Li[1*]

Abstract

Background This study aimed to describe the color Doppler flow features of papillary thyroid carcinoma (PTC) and to further investigate the associations between these features and lymph node metastasis (LNM).

Methods A retrospective analysis of the clinical data of 287 PTC patients confirmed by postoperative pathology at the Second Affiliated Hospital of Xi'an Jiaotong University from January 2022 to April 2023 was conducted. The Adler grading system and novel blood flow patterns were used to analyze the vascularity of the PTC lesions on color Doppler images. Univariate and multivariate logistic regression analyses were conducted to evaluate the independent effects of blood flow characteristics on LNM, and a logistic regression model was established to assess their predictive value for PTC-related LNM.

Results In all, 287 PTC lesions were analyzed using color Doppler ultrasonography, which identified five main reference patterns: avascular (26.13%), dot-line (24.74%), branching (14.29%), garland (11.50%), and rich-disorganized (23.34%). The Adler blood flow grading was as follows: 0 (32.75%), I (18.82%), II (19.16%), and III (29.27%). A univariate analysis revealed that the Adler grade was not significantly associated with LNM ($P > 0.05$), whereas the garland pattern was significantly associated with LNM ($P < 0.05$). A multivariate analysis revealed that the garland pattern was an independent protective factor for LNM (OR [95% CI] = 0.386 [0.156–0.893]). The incorporation of the garland pattern into the model improved the predictive accuracy for LNM in PTC patients, and the AUC increased from 0.727 [95% CI: 0.669–0.786] to 0.767 [95% CI: 0.731–0.821].

Conclusions This study classifies PTC into five types on the basis of color Doppler flow features and highlights the garland pattern as a potential predictor of LNM risk.

Keywords Color Doppler ultrasound, Papillary thyroid carcinoma, Lymphatic metastasis, Blood flow

*Correspondence:
Hua Wang
wanghua37@xjtu.edu.cn
Xiaopeng Li
lixiaopeng123@xjtu.edu.cn
[1]Department of Ultrasound, The Second Affiliated Hospital of Xi'an Jiaotong University, 157 Xiwu Road, Xi'an, Shaanxi Province 710004, China
[2]Department of Ultrasound, Ankang Central Hospital, Ankang, Shaanxi Province 725000, China

Background

Thyroid cancer is the most common endocrine malignancy, and papillary thyroid carcinoma (PTC) accounts for approximately 80% of all thyroid cancers [1, 2]. Although PTC lesions are generally indolent, lymph node metastasis (LNM) can occur in the early stage of the disease and is correlated with local recurrence and a poor prognosis [3]. The neovascularization process is critical to tumor growth and metastasis [4]. Color Doppler ultrasound (CDUS), an economical, simple, and noninvasive imaging tool, has been widely used for the assessment of tumor vascularity and blood flow characteristics. Therefore, a deeper analysis of the CDUS imaging features of PTC and their relationship with LNM can not only aid in the early diagnosis of PTC but can also provide a basis for assessing the risk of LNM, thus facilitating personalized disease management decisions.

Although numerous studies have used CDUS to assess blood flow in PTC, the characteristics of blood flow remain an ongoing area of research and debate [5–7], and a widely accepted and standardized classification system has yet to be established. Commonly used blood flow grading systems, such as the Lagalla [8] and Adler [9] classifications, are designed primarily for the evaluation of thyroid nodules and do not fully account for the unique blood flow features of PTCs. As a result, these grading systems may have certain limitations when applied to the blood flow assessment of PTC, particularly regarding the accurate identification of high-risk lesions with LNM, which could affect the precision of clinical decision-making. Although some studies have revealed the specific manifestations of blood flow in PTC [10, 11], these studies have failed to cover its diversity. To date, we still lack a classification method that can comprehensively reflect the blood flow features of PTC, which limits the clinical application of blood flow features in predicting the risk of LNM.

Therefore, this study aims to systematically summarize the sonographic features of PTC under CDUS and to explore the relationship between blood flow patterns and LNM. By introducing a new blood flow classification system, we hope to provide a novel imaging reference for assessing the invasiveness of PTC and predicting the risk of LNM.

Materials and methods

Study subjects

We reviewed the medical records of thyroid cancer patients who were admitted to the Second Affiliated Hospital of Xi'an Jiaotong University between January 2022 and April 2023. In all, 287 patients with 287 lesions were included in the study. The largest lesion in each patient was selected for analysis. Among the 287 patients, 70 were male (24.4%), with ages that ranged from 18 to 65 years (mean age 43.7 ± 10.6 years), while 217 were female (75.6%), with ages that ranged from 10 to 77 years (mean age 45.2 ± 12.3 years). The inclusion criteria were as follows: successful total or partial thyroidectomy; functional neck lymphadenectomy or radical lymphadenectomy; a diagnosis of PTC confirmed by postoperative pathology; and complete preoperative ultrasound images and clinical data. The exclusion criteria were as follows: the presence of other malignant tumors; a history of fine needle aspiration (FNA) before ultrasound examination in our hospital; a history of radiotherapy or chemotherapy; and lymphadenopathy due to different factors. This study was approved by the Hospital Ethics Committee (no. 2023503). Informed consent was obtained from all patients, and all ethical issues were strictly respected.

Equipment and data collection

Ultrasound examinations were performed with the Hitachi Ascendus ultrasound diagnostic system with an EUP-L75 probe operating at a frequency range of 5–18 MHz. Preoperative ultrasound scans were conducted by a senior physician (with 15 years of experience) in the Department of Ultrasound. The patient was placed in a supine position with a pillow placed under the neck to achieve slight hyperextension. Both transverse and longitudinal scans of the bilateral thyroid lobes and isthmus were performed to acquire multiple grayscale ultrasound and CDUS images of the thyroid lesions. The ultrasound system was preset for thyroid examination, and adjustments were made to the depth, gain, and focus, as necessary, to optimize image quality. The grayscale ultrasound features, including size, composition, echogenicity, shape, margins, and echogenic foci, were recorded according to the ACR TI-RADS lexicon. CDUS images were obtained by fine-flow imaging technology. This advanced imaging technique, which differs from conventional color Doppler, allows for the detection of low-velocity blood flow and small vessels. This technique also improves image quality by reducing common artifacts through optimized signal processing algorithms. The physical settings for color Doppler imaging were a low-pass filter, a Doppler gain set to 80–90, and a velocity scale adjusted to approximately 1.5–2.5 cm/s. During the procedure, the operator avoided the application of pressure on the lesions to prevent interference with the blood flow signals. All color Doppler images were exported in JPEG format. Patient data, including age and sex, were collected from the medical records. The number of lesions, HT status, and LNM status were confirmed through pathological findings.

Analysis of CDUS imaging characteristics

We systematically analyzed CDUS images of 287 lesions. Blood flow was classified according to the Adler grading system, as follows: Grade 0 (avascular): no detectable

flow; Grade I (minimal): 1–2 flow pixels; Grade II (moderate): one main vessel or several small vessels; Grade III (marked): ≥4 distinct vessels [9]. Furthermore, two senior sonographers with >10 years of thyroid imaging experience independently categorized the images into five predominant vascular patterns through meticulous observation and clinical experience, with a focus on vascular morphology, spatial distribution, and flow abundance. The key features of each pattern were thoroughly discussed until a consensus was reached. The five patterns included the following: avascular: no visible blood flow signal; dot-line: small local blood flow signals appearing as dots or short rods; branching: vessels appear in a branching pattern, extending toward the center of the lesion; garland: blood flow signals radiate concentrically at the lesion's edge, with little to no blood flow in the center; and rich-disorganized type: dense, irregular, and chaotic blood flow signals within the lesion. To minimize observer bias, we implemented a rigorous dual-blind validation protocol. Both readers conducted retrospective, independent analyses, with initial concordance achieved in 84.3% of the cases ($\kappa = 0.80$, $p < 0.001$). Discordant interpretations (15.7%) were resolved through joint re-evaluation with reference to established diagnostic criteria. The subjective classification flowchart of blood flow patterns is shown in Fig. 1.

Statistical methods

In this study, statistical analyses were performed using SPSS version 27.0 (IBM, Armonk, NY, USA) and R software (version 4.3.2). Continuous variables are expressed as the mean ± standard deviation ($\bar{X} \pm S$), and categorical variables are presented as frequencies (n, %). For continuous variables with a normal distribution, comparisons between two groups were made using independent samples t-tests, and comparisons among multiple groups were made using one-way analysis of variance (ANOVA). For nonnormally distributed continuous variables, the Mann–Whitney U test was used for two-group comparisons, and the Kruskal–Wallis H test was used for comparisons among multiple groups. Multivariate logistic regression was performed to analyze the risk factors for LNM. In the multivariate regression analysis, LNM was set as the dependent variable, and variables with statistical significance in the univariate and multivariate analysis were included as independent variables. To assess the predictive value of the garland blood flow pattern, we constructed logistic regression models that included and excluded the garland pattern. Mode l evaluation included decision curve analysis (DCA) and calibration curves as well as the sensitivity, specificity, accuracy, positive predictive value (PPV), and negative predictive value (NPV). Additionally, nomograms were used to visualize the best model, and DeLong's test was applied to compare the differences in the ROC curves of different models. Unless otherwise specified, a significance level of $\alpha = 0.05$ was used for all tests.

Results

General information and ultrasonic characteristics

The clinical data and ultrasound characteristics of the patients are detailed in Table 1. The detection rate of blood flow signals by CDUS was 73.9% (212/287). The 287 lesions were classified into five categories according to the new blood flow classification system proposed in this study: avascular (26.13%), dot-line (24.74%),

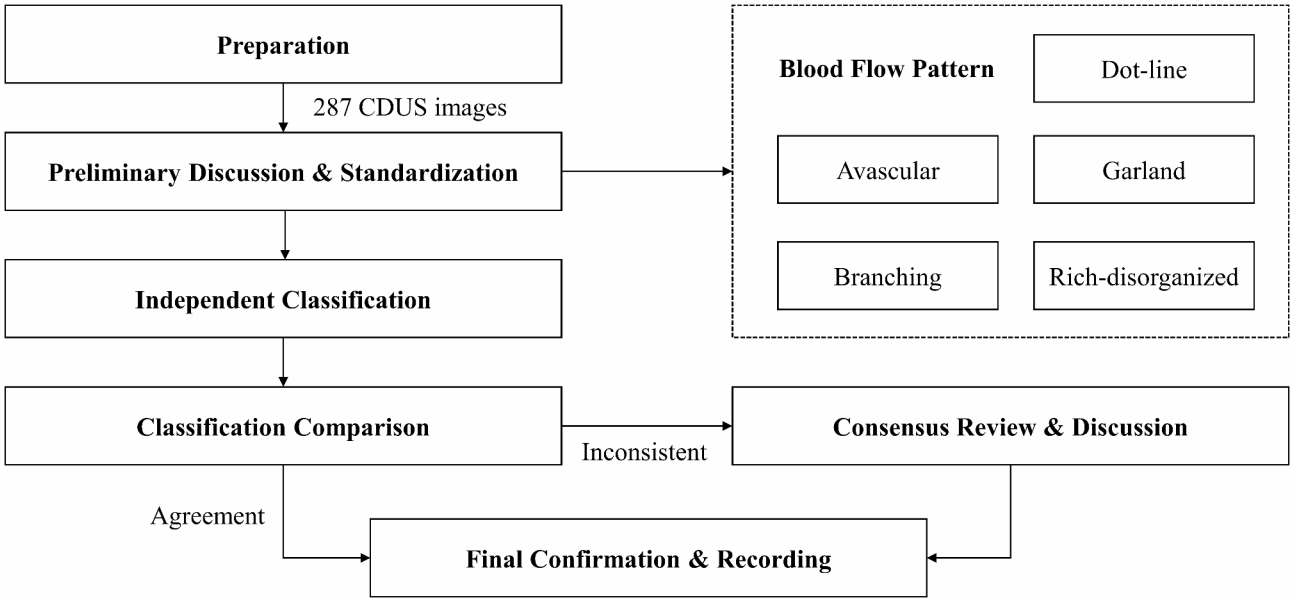

Fig. 1 Flowchart of the classification process of blood flow patterns in PTC

Table 1 Descriptive analysis and analysis of differences in the baseline characteristics of 287 patients with PTC

Variable	*n*(%)	LNM status		Statistic	*P* value
		No (*n* = 142)	Yes (*n* = 145)		
Age	44.82 ± 11.94	48.89 ± 10.63	40.83 ± 11.84	$t = 6.06$	< 0.001*
Tumor diameter	11.14 ± 7.64	8.78 ± 4.04	13.45 ± 9.43	t=-5.43	< 0.001*
Sex				$\chi^2 = 4.41$	0.036*
Female	217(75.61)	115(53.00)	102(47.00)		
Male	70(24.39)	27(38.57)	43(61.43)		
Composition				-	0.976
Mixed cystic and solid	8(2.79)	4(50.00)	4(50.00)		
Solid or almost completely solid	279(97.21)	138(49.46)	141(50.54)		
Echogenicity				-	0.496
Hyperechoic or isoechoic	10(3.48)	4(40.00)	6(60.00)		
Hypoechoic	273(95.12)	135(49.45)	138(50.55)		
Very hypoechoic	4(1.39)	3(75.00)	1(25.00)		
Shape				$\chi^2 = 2.94$	0.087
Taller than wide	113(39.37)	63(55.75)	50(44.25)		
Wider than tall	174(60.63)	79(45.40)	95(54.60)		
Margin				$\chi^2 = 4.27$	0.118
Ill-defined	211(73.52)	112(53.08)	99(46.92)		
Lobulated or irregular	40(13.94)	15(37.50)	25(62.50)		
Extra-thyroidal extension	36(12.54)	15(41.67)	21(58.33)		
Echogenic Foci				-	0.640
None or large comet-tail artifacts	172(59.93)	88(51.16)	84(48.84)		
Macrocalcifications	31(10.80)	17(54.84)	14(45.16)		
Peripheral calcifications	3(1.05)	1(33.33)	2(66.67)		
Punctate echogenic foci	81(28.22)	36(44.44)	45(55.56)		
HT status				$\chi^2 = 1.80$	0.179
No	218(75.96)	103(47.25)	115(52.75)		
Yes	69(24.04)	39(56.52)	30(43.48)		
Number of lesions				$\chi^2 = 6.53$	0.011*
Single	181(63.07)	100(55.25)	81(44.75)		
Multiple	106(36.93)	42(39.62)	64(60.38)		
Blood flow type				$\chi^2 = 5.60$	0.231
Avascular	75(26.13)	36(48.00)	39(52.00)		
Dot-line	71(24.74)	36(50.70)	35(49.30)		
Branching	41(14.29)	20(48.78)	21(51.22)		
Garland	33(11.50)	22(66.67)	11(33.33)		
Rich-disorganized	67(23.34)	28(41.79)	39(58.21)		
Adler blood flow grade				$\chi^2 = 2.62$	0.455
0	94(32.75)	48(51.06)	46(48.94)		
I	54(18.82)	27(50.00)	27(50.00)		
II	55(19.16)	31(56.36)	24(43.64)		
III	84(29.27)	36(42.86)	48(57.14)		

- represent the Fisher's exact test; * represent P < 0.05; HT: Hashimoto's thyroiditis; LNM: lymph node metastasis; PTC: papillary thyroid carcinoma

branching (14.29%), garland (11.50%), and rich-disorganized (23.34%) (Fig. 2). According to the Adler grading system, the lesions were classified into four levels: Grade 0 (32.75%), Grade I (18.82%), Grade II (19.16%), and Grade III (29.27%) (Fig. 3).

Analysis of variations in PTC lesion size by blood flow type

Lesion size is regarded as an important factor that predicts the invasiveness of PTC and the risk of LNM [12]. Thus, we analyzed the differences in lesion size across different blood flow types. Table 2 shows marked differences in the sizes of the lesions with different blood flow types ($P < 0.001$). The pairwise comparison demonstrated that the lesions with dot-line, branching, and

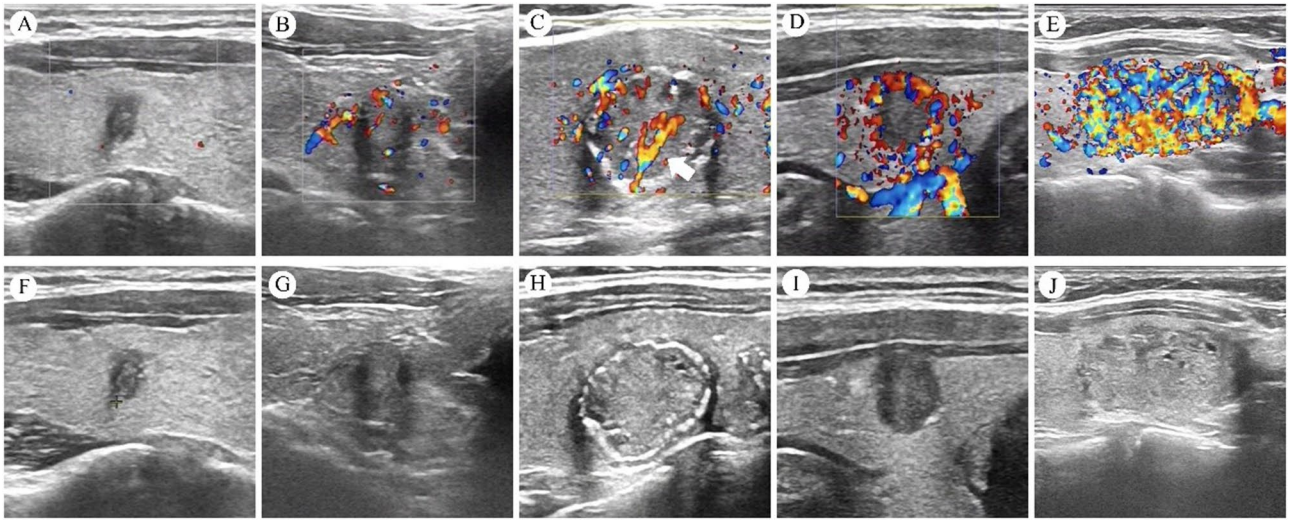

Fig. 2 Color Doppler (top) and grayscale (bottom) ultrasound images of the five blood flow patterns. **A** avascular pattern showing no significant blood flow around or within the lesion. **B** dot-line pattern showing spot and short rod vessels around or inside the lesion. **C** branching pattern showing long blood vessels (indicated by white arrows), nearly or exceeding the lesion's radius, and extending the lesion in a radial arrangement. **D** garland pattern showing red and blue blood flow signals concentrated around the focal area, with no central blood flow. **E** rich-disorganized pattern showing dense red and blue blood flow signals visible, with disordered intratumoral vessels connected

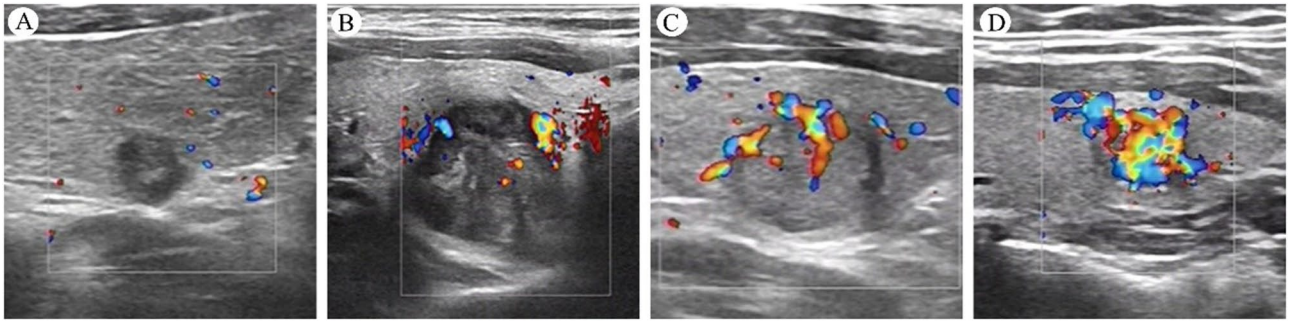

Fig. 3 Illustration of the four-grade blood flow signal classification according to the Adler grading system. **A**: absent vascularity (grade 0). **B**: minimal vascularity (grade I). **C**: moderate vascularity (grade II). **D**: marked vascularity (grade III)

Table 2 Analysis of lesion size variations in 287 PTCs by blood flow type

Pattern	*N*	Tumor diameter(mm)	Z	*P* value
Avascular	75	7.93 ± 3.70		
Dot-line	71	10.56 ± 5.59a		
Branching	41	11.83 ± 6.94a	39.708	0.000
Garland	33	9.53 ± 4.18		
Rich-disorganized	67	15.74 ± 11.47abc		

a: $P<0.05$(compared with avascular pattern); b: $P<0.05$ (compared with dot-line pattern); c: $P<0.05$ (compared with garland pattern)

rich-disorganized blood flow were significantly larger than those without blood flow ($P<0.05$). The lesions with rich-disorganized blood flow were significantly larger than those with dot-line and branching patterns ($P<0.05$).

Construction and results of the multivariate logistic regression model

The 287 PTC patients were divided into the cervical LNM group ($n=145$, 50.52%) and the noncervical LNM group ($n=142$, 49.48%). The univariate analysis revealed significant differences in patient age, tumor diameter, number of lesions, and sex according to LNM status ($P<0.05$). No statistically significant differences were found for the other factors ($P>0.05$) (Table 1). In the multivariate logistic regression analysis with LNM as the dependent variable, age, tumor diameter, number of lesions, and the garland pattern were significantly associated with LNM ($P<0.05$), whereas sex was not significantly associated ($P>0.05$) (Table 3). Variables with statistical significance in both the univariate and multivariate analyses were included in the final model. In Model 1, age (OR [95% CI] = 0.938 [0.915–0.961]) and the garland pattern (OR [95% CI] = 0.386 [0.156–0.893]) were protective factors for LNM, whereas tumor diameter (OR [95% CI] = 1.116

Table 3 Multivariate analyses of factors associated with LNM in PTC

Variable	B	SE	Wald	*P*	OR	OR 95% CI
Age	-0.064	0.013	25.808	0.000	0.938	0.915 ~ 0.961
Tumor diameter	0.110	0.026	17.375	0.000	1.116	1.060 ~ 1.175
Number of lesions	0.746	0.283	6.941	0.008	2.108	1.210 ~ 3.672
Sex	0.496	0.318	2.431	0.119	1.642	0.880 ~ 3.062
Garland pattern	-0.890	0.442	4.044	0.044	0.411	0.173 ~ 0.978
Intercept	0.697	0.729	0.915	0.339	2.008	

Table 4 Multivariate logistic regression results for LNM in PTC patients

Model	Characteristics	B	SE	Z	*P*	OR	95% CI
Model1	Age	-0.064	0.013	-5.132	< 0.001	0.938	0.915 ~ 0.961
	Tumor diameter	0.110	0.026	4.196	< 0.001	1.116	1.063 ~ 1.179
	Number of lesions	0.727	0.281	2.585	0.009	2.069	1.210 ~ 3.672
	Garland pattern	-0.953	0.442	-2.163	0.031	0.386	0.156 ~ 0.893
	Intercept	1.689	0.895	1.206	0.227	2.373	
Model2	Age	-0.061	0.013	-4.952	< 0.001	0.941	0.917 ~ 0.964
	Tumor diameter	0.112	0.026	4.278	< 0.001	1.118	1.066 ~ 1.181
	Number of lesions	0.746	0.277	2.688	0.007	2.110	1.230 ~ 3.662
	Intercept	0.550	0.689	0.789	0.430	1.734	

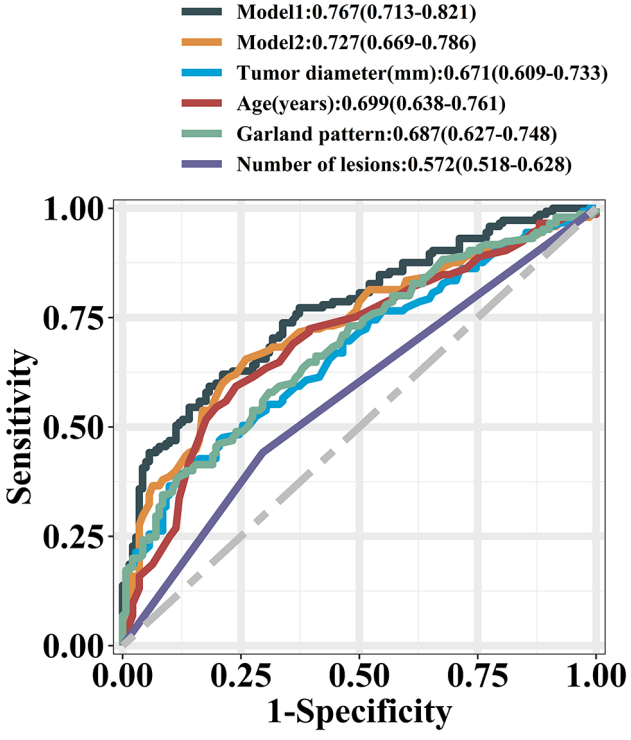

Fig. 4 ROC curve of the logistic regression model for the prediction of LNM. Model 2 includes the variables age, tumor diameter (mm), and number of lesions, while Model 1 includes the Garland pattern on the basis of Model 2. 95% CI For Model 1 and Model 2 (95% CI difference): 0.0005–0.0792, Z = 1.988, *P* = 0.047

[1.063–1.179]) and lesion number (OR [95% CI] = 2.069 [1.210–3.672]) were risk factors for LNM. Model 2 was similar, as age (OR [95% CI] = 0.941 [0.917–0.964]) still served as a protective factor for LNM, but tumor diameter (OR [95% CI] = 1.118 [1.066–1.181]) and lesion number (OR [95% CI] = 2.110 [1.230–3.662]) were risk factors for LNM (Table 4). The ROC curves of Model 1 (AUC, 95% CI = 0.767, 0.731–0.821) and Model 2 (AUC, 95% CI = 0.727, 0.669–0.786) were compared using the DeLong test. The results indicated that the inclusion of the garland pattern in Model 1 significantly improved its discriminatory ability compared with when the garland pattern was excluded (Fig. 4). With respect to the other model performance metrics, the best model, Model 1, had an accuracy of 0.704 (95% CI, 0.702–0.705), a sensitivity of 0.693 (95% CI, 0.513–0.773), a specificity of 0.817 (95% CI, 0.753–0.881), a positive predictive value of 0.768 (95% CI, 0.690–0.846), a negative predictive value of 0.663 (95% CI, 0.593–0.733), and a cutoff value of 0.573. The results of the other models and the univariate analysis are also presented in Fig. 4; Table 5.

Prediction nomogram for LNM in PTC and its validation

On the basis of the aforementioned results, we plotted the clinical decision curve, calibration curve, and nomogram for the optimal model. In the DCA, the vertical axis represents the net benefit, whereas the horizontal axis represents the risk threshold. The results show that when the risk threshold is approximately 0.2, the red curve corresponding to the nomogram model (Model 1) consistently lies above both the "all" model and the "none" model. This finding indicates that the model incorporating the garland pattern provides a greater net benefit at this risk threshold, which suggests its potential clinical application value (Fig. 5). The calibration curve, in which the predicted values closely overlapped with the 45° line, demonstrated excellent calibration, which indicates that the model's predictions closely aligned with the actual

Table 5 Model performance metrics for the prediction of LNM in PTC

Model	Cutoff	Accuracy (95%CI)	Sensitive (95%CI)	Specificity (95%CI)	Positive Predictive Value (95%CI)	Negative Predictive Value (95%CI)
Tumor diameter(mm)	0.568	0.634(0.633–0.636)	0.414(0.334–0.494)	0.859(0.802–0.916)	0.750(0.655–0.845)	0.589(0.522–0.656)
Age(years)	0.557	0.676(0.674–0.677)	0.593(0.513–0.673)	0.761(0.690–0.831)	0.717(0.636–0.797)	0.647(0.574–0.719)
Garland pattern	0.430	0.544(0.542–0.545)	0.924(0.881–0.967)	0.155(0.095–0.214)	0.528(0.466–0.589)	0.667(0.506–0.828)
Number of lesions	0.526	0.571(0.570–0.573)	0.441(0.361–0.522)	0.704(0.629–0.779)	0.604(0.511–0.697)	0.552(0.480–0.625)
Model2	0.422	0.700(0.699–0.702)	0.593(0.727–0.859)	0.606(0.525–0.686)	0.673(0.602–0.743)	0.741(0.662–0.821)
Model1	0.573	**0.704(0.702–0.705)**	**0.693(0.513–0.773)**	**0.817(0.753–0.881)**	**0.768(0.690–0.846)**	0.663(0.593–0.733)

Model 2 includes variables Age, Tumor diameter(mm) and Number of lesions

Model 1 adds Garland pattern on the basis of Model, Bold values indicate the best-performing model under the same evaluation criteria

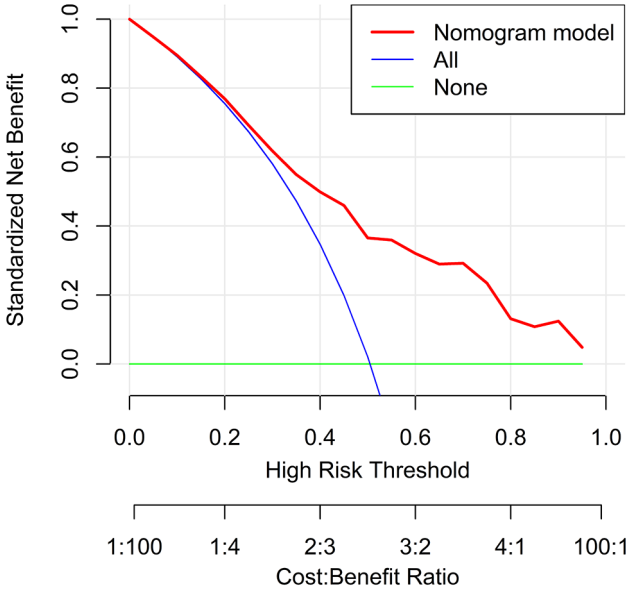

Fig. 5 Clinical decision curve analysis. The x-axis shows the high-risk threshold, and the y-axis shows the net benefit

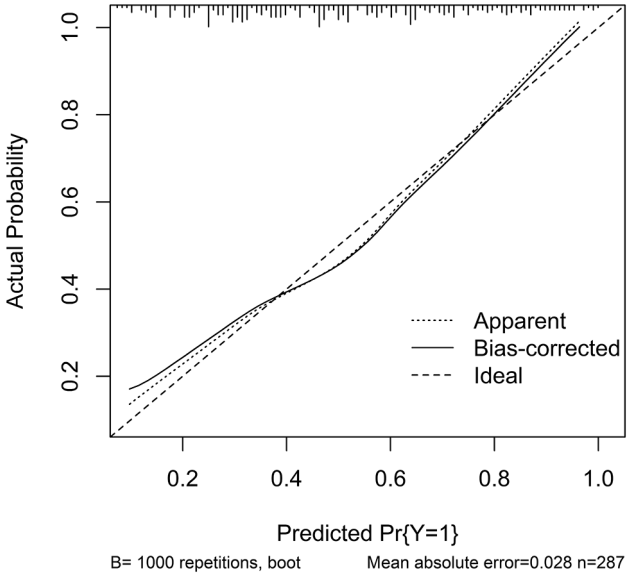

Fig. 6 Bootstrap method. The x-axis shows the probability of LNM status predicted by the nomogram, and the y-axis shows the actual ratio of the LNM status. The reference line is dashed, indicating apparent calibration

outcomes (Fig. 6). The nomogram visually represents the regression coefficients from Model 1 shown in Table 4 (Fig. 7).

Discussion

This study presents a novel blood flow classification system to describe the blood flow characteristics of PTC and explores the role of these features in predicting LNM in PTC patients. Our findings indicate that among the five blood flow patterns, the garland pattern is an independent protective factor for LNM (OR [95% CI] = 0.386 [0.156–0.893]). Furthermore, we observed that the inclusion of the garland pattern significantly improved the predictive accuracy for LNM in conventional PTC models, as the AUC increased from 0.727 [95% CI: 0.669–0.786] to 0.767 [95% CI: 0.731–0.821], a change that was statistically significant ($p < 0.05$, DeLong's test).

Ultrasound is the preferred imaging method for the diagnosis of thyroid cancer [13]. Several national and international professional organizations have developed risk stratification systems for use in ultrasound [14]. However, the present RSSs for thyroid nodules are based on grayscale ultrasound, and CDUS has not been widely adopted as a complementary technique [15]. This is primarily because numerous studies of CDUS for thyroid nodules have reported mixed conclusions. The mixed conclusions reported in these studies were primarily the result of differences in Doppler parameters and the classification of blood flow. "Abundant blood flow within the nodule" as an indicator of malignancy was removed from the 2015 ATA [16] guidelines on the basis of a large study by Moon [17], which revealed that PTC lesions often lack blood flow, thus questioning the diagnostic value of color Doppler flow imaging. However, Chammas [18] argued that shortcomings in Moon's research methods might have underestimated the effectiveness of color Doppler flow imaging. In our study, we employed fine-flow imaging technology with settings of a low-wall filter, a Doppler gain of 80–90, and a velocity scale of 1.5–2.5 cm/s. During the procedure, we ensured that minimal pressure was

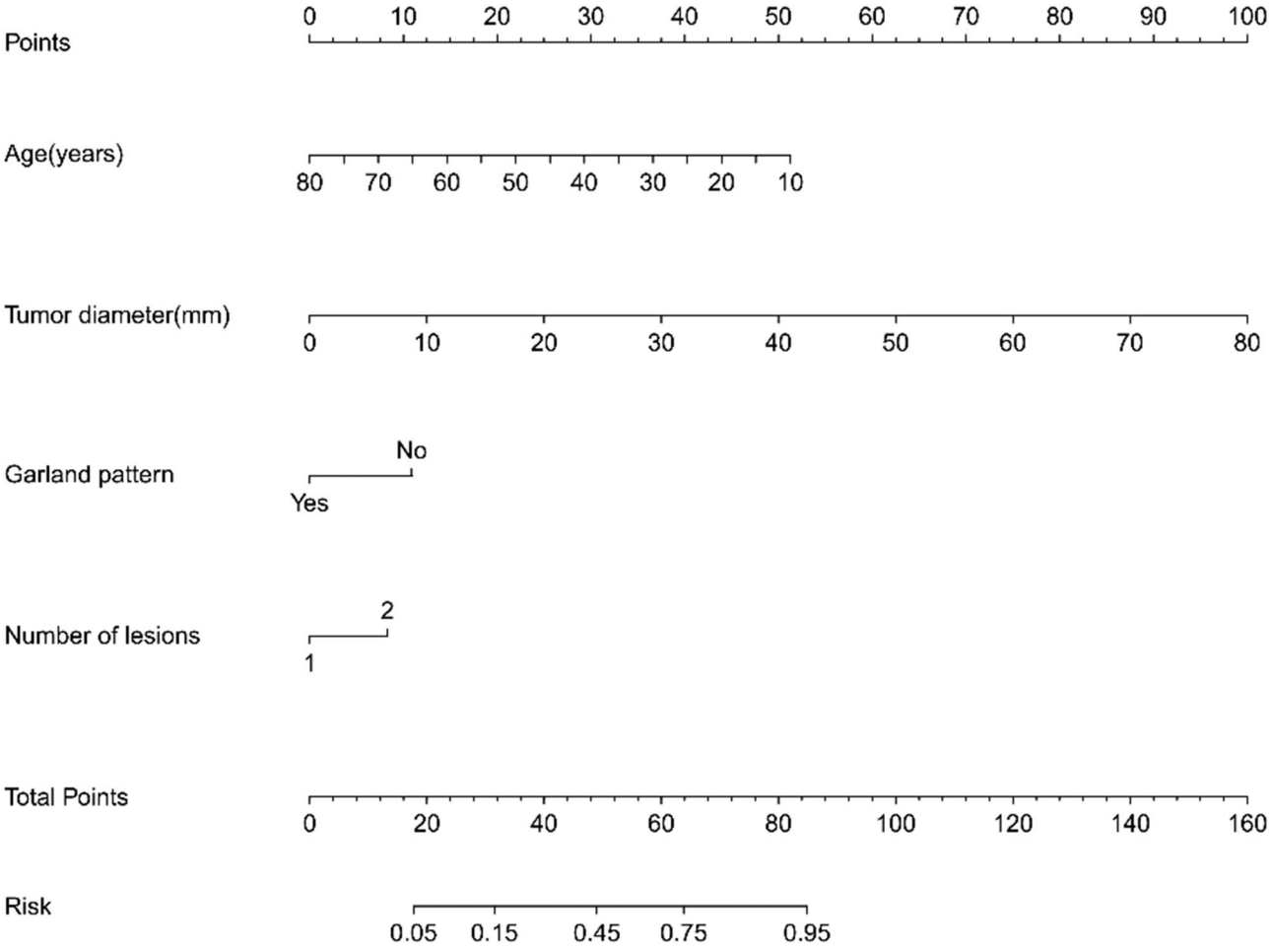

Fig. 7 Nomogram for predicting the risk of LNM status. The linear predictor is the coordinate axis of the linear prediction value, which is transformed into the corresponding probability value through a conversion function

applied to the probe, as even slight pressure can obscure low-velocity blood flow. The blood flow detection rate was 73.9% (212/287), which demonstrates that, under appropriate parameter settings and when performed by experienced operators, fine-flow imaging can reliably assess the blood flow characteristics of PTC lesions.

The Adler blood flow classification system, originally designed to assess blood flow within breast tissue lesions, aims to quantify blood supply. Although this system was not specifically developed for thyroid diseases, many researchers still use it to describe blood flow characteristics in thyroid cancer patients. In our study, we applied the Adler classification to CDUS images of 287 PTC patients. The results revealed that 139 lesions (48.43%) presented a rich blood supply, whereas 148 lesions (51.56%) presented a poor blood supply. The univariate analysis revealed no significant correlation between Adler's blood flow grade and LNM in PTC patients ($P > 0.05$). These findings suggest that the Adler classification system does not adequately reflect the blood flow characteristics of PTC lesions and has limited clinical value in the assessment of PTC. In 1993, Lagalla [8] proposed the following blood flow classification of thyroid nodules on the basis of the spatial distribution of blood vessels: no appreciable glandular flow (I); presence of signals in perinodular locations (II); and perinodular and intranodular flow (III). Chammas [19] and many other scholars later refined the classification to include vascularity. Most current systems used to describe blood flow in thyroid cancer are essentially variations of Lagalla's original framework, and significant differences in results have been reported across studies. As a result, these existing classification systems have not been formally incorporated into clinical practice guidelines. The lack of consensus and standardization in PTC blood flow classification has hampered the widespread clinical application of these systems. With advancements in research, some scholars have proposed characteristic blood flow patterns in PTC lesions. Xue N [10] noted that the wheel sign on CDUS is highly specific for PTCs. Lacout A [11] observed that penetrating "sword-like" vessels observed on CDUS images may be present in poorly differentiated papillae

at an early stage. These studies suggest that PTC exhibits distinct characteristics on CDUS images. However, our understanding of the blood flow characteristics of PTC is still incomplete. The color Doppler imaging of PTCs is complex and varied, but certain patterns are observed. On the basis of extensive clinical observations and analysis of the images collected in this study, we propose a new blood flow classification system (Fig. 2). Unlike previous systems, the new classification system more comprehensively depicts the characteristics of PTC on CDUS. We emphasize the integration of blood flow morphology, and thus it is easier for observers to remember and clearly distinguish different patterns. Notably, the five distinct patterns reflect different aspects of tumor neovascularization and provide an important foundation for further evaluating the relationship between blood flow features and LNM risk.

Color Doppler flow imaging can reveal the characteristics of the internal circulatory system of PTC lesions in different pathological environments. A significant correlation was revealed between the vascular structure of papillary carcinoma and the characteristics of color Doppler images [20]. The rich-disorganized pattern is characterized by abnormal anastomosis of rich blood vessels and the irregular aggregation of locally twisted small blood vessels into "glomerular" structures, which may be the product of tumor neovascularization, while distorted blood vessels may be caused by tumor cell proliferation and extrusion [21, 22]. The branching pattern is characterized by a large vegetative vessel on the outside that penetrates the lesion, which may be related to tumor-host vascular co-selection or angiogenesis. Perforation throughout the tubercle indicates poorly differentiated papillary or anaplastic thyroid nodules at an early stage [11]. The garland pattern is characterized by dense and small perforating branches at the edges, which may be the result of angiogenesis in thyroid cancer, rather than the proliferation of fibrous tissue or scar formation within the tumor that pulls the surrounding host blood vessels [23]. Some scholars have reported that typical PTC and high-cell PTC are characterized by intratumoral blood vessels that connect to form several anastomoses, that sclerotic PTC is poorly vascularized, and that follicular PTC is characterized by small intratumoral branches, frequent anastomosis, and a lack of central large blood vessels [24]. These findings suggest that CDUS blood flow characteristics may be helpful in the differentiation of thyroid papillary carcinoma subtypes. Nevertheless, as angiogenesis is a multifaceted process governed by various cellular factors, the vascular characteristics observed on CDUS images likely arise from a combination of factors. Consequently, obtaining compelling evidence to elucidate the molecular mechanisms underlying blood supply characteristics necessitates more intricate experimental studies.

Angiogenesis and the proliferation of abnormal blood vessels are frequently associated with tumor cell proliferation [25]. In this study, different blood flow patterns were observed in lesions of different sizes (Table 2). Specifically, larger lesions tended to exhibit more abundant and disorganized internal blood flow. This finding aligns with that of Fukuoka et al., who reported that highly vascularized lesions in PTC patients grow significantly faster than those with less vascularization [26]. This consistency underscores the relationship between blood flow characteristics and tumor growth, which reinforces the clinical relevance of evaluating blood flow patterns for the prediction of PTC aggressiveness. A study involving 748 patients demonstrated that primary tumor size is an independent risk factor for cervical LNM [27]. Our study also confirmed that lesion size is an independent risk factor for LNM. However, the univariate analysis revealed no significant correlation between a disorganized blood flow pattern and LNM ($P > 0.05$), possibly because of the common occurrence of lymphatic invasion in PTC [28]. In contrast, a significant association was observed between the garland pattern and LNM ($P < 0.05$). Previous research has identified radiating blood flow as a novel ultrasonographic feature of thyroid cancer [29], and the garland pattern observed in our study is highly consistent with one of the radiating blood flow characteristics described in that study. Given the significant correlation between the garland blood flow pattern and LNM, we further performed a multivariate logistic regression analysis. The results indicated that the garland blood flow pattern is an independent protective factor for LNM (OR [95% CI] = 0.386 [0.156–0.893]), which suggests its potential role in predicting LNM in PTC. To validate its predictive value, we integrated this pattern into a regression prediction model. ROC curve analysis demonstrated that Model 1 (AUC = 0.767) had superior discriminative ability in predicting LNM compared with Model 2 (AUC = 0.727). The DeLong test confirmed that the inclusion of the garland blood flow pattern significantly improved the model's performance, which highlights its unique value in LNM prediction. Figure 7 visualizes the regression system of Model 1 as shown in Table 4. These findings indicate that younger age, larger tumor size, nongarland blood flow, and multifocality are high-risk factors for LNM. Clinicians can utilize this model by assessing relevant high-risk factors in patients to calculate a risk score and estimate the probability of LNM. Angiogenesis is a crucial component of the tumor ecosystem and plays a significant role in tumor biology. In this study, the 33 PTC lesions with garland blood flow exhibited minimal internal vascularization, with a maximum diameter of 19 mm. Previous studies have

suggested that tumors lacking a sufficient vascular supply typically do not exceed 20 mm in diameter [30]. Without continuous recruitment of new capillaries, tumors are generally unable to grow beyond a microscopic size of 1–2 mm^3 [31]. While insufficient intratumoral vascularization may explain the restricted tumor growth, it does not fully account for the lower risk of LNM. Currently, the underlying mechanism of garland blood flow formation remains unclear. Future studies may clarify this mechanism and potentially lead to important discoveries.

Xiaohong Jia et al. developed a human artificial intelligence hybrid (HAIbrid) framework for thyroid nodule malignancy stratification and diagnosis and identified a second-order interactive feature—vertically distributed blood flow signals surrounding the nodule—that has been overlooked by radiologists and traditional feature selection methods [32]. This feature closely resembles the garland pattern observed in our study. Its incorporation significantly improved the model's AUC, which demonstrates the potential of pattern-based classification methods in medical imaging. Similarly, research by Burak Taşcı confirmed that pattern-based classification enhances diagnostic accuracy and efficiency because of the automatic extraction and analysis of critical imaging features [33]. The garland pattern proposed in our study, as a pattern-based classification feature, holds significant potential for predicting LNM in PTC. The integration of artificial intelligence techniques could further optimize predictive models and provide robust support for clinical diagnosis.

While the findings of this study are encouraging, several limitations should be acknowledged. First, as a single-center, retrospective study, selection bias is unavoidable. While the sample size is sufficient to support our analysis, the generalizability of the results requires further validation through multicenter studies with larger cohorts. Second, the quality of ultrasound images is influenced by the operator's skill and experience, and blood flow classification relies on subjective interpretation. The integration of advanced technologies, such as artificial intelligence and machine learning models, may help overcome these limitations.

Conclusion

In conclusion, PTC lesions present certain characteristics on CDUS images, and blood flow can be divided into five patterns: avascular, dot-line, branching, garland, and rich-disorganized. The discovery of the garland pattern provides a novel tool for predicting LNM risk, aiding clinicians in making more accurate assessments of tumor aggressiveness. Further exploration and research on the blood flow characteristics of PTC will provide crucial imaging insights to support personalized treatment and follow-up management.

Abbreviations

PTC	Papillary thyroid carcinoma
LNM	Lymph node metastasis
HT	Hashimoto's thyroiditis
CDUS	Color Doppler ultrasound
mm	Millimeter

Acknowledgements

We deeply appreciate the ultrasonographers who contributed to the research process, and we are grateful to the surgeons who helped and the pathologists who assisted in the diagnosis.

Author contributions

Lu Cao conceived of the project and wrote the manuscript text. Xiangru Wang carried out the literature search. Ying Cao and Fangxi Zhao are responsible for figures processing. Xinxin Lu and Lei Sun participated in its design and coordination. Hua Wang and Xiaopeng Li are responsible for project administration and funding acquisition. All authors reviewed the manuscript.

Funding

This study has received funding from the Key Research and Development Program of Shaanxi Province, China (2020GXLH-Y-002). The funding bodies played no role in the design of the study and collection, analysis, and interpretation of data and in writing the manuscript.

Data availability

The data that support the findings of this study are available on request from the corresponding author upon reasonable request.

Declarations

Ethics approval and consent to participate

This study was approved by the Medical Ethics Committee of the Second Affiliated Hospital of Xi'an Jiaotong University, with the approval number 2023503. All experiments involving human participants were conducted in strict accordance with relevant guidelines and regulations. Informed consent was obtained from all participants involved in this study.

Consent for publication

Not applicable.

Competing interests

The authors declare no competing interests.

Received: 17 November 2024 / Accepted: 25 February 2025
Published online: 06 March 2025

References

1. Chen DW, Lang BHH, McLeod DSA, Newbold K, Haymart MR. Thyroid cancer. Lancet. 2023;401(10387):1531–44.
2. Siegel RL, Miller KD, Wagle NS, Jemal A. Cancer statistics, 2023. CA Cancer J Clin. 2023;73(1):17–48.
3. Yu J, Deng Y, Liu T, Zhou J, Jia X, Xiao T, Zhou S, Li J, Guo Y, Wang Y. et al. Lymph node metastasis prediction of papillary thyroid carcinoma based on transfer learning radiomics. Nat Commun. 2020;11(1):4807.
4. Skuletic V, Radosavljevic GD, Pantic J, Markovic BS, Jovanovic I, Jankovic N, Petrovic D, Jevtovic A, Dzodic R, Arsenijevic N. Angiogenic and lymphangiogenic profiles in histological variants of papillary thyroid carcinoma. Pol Arch Intern Med. 2017;127(6):429–37.
5. Mandel SJ. Diagnostic use of ultrasonography in patients with nodular thyroid disease. Endocr Pract. 2004;10(3):246–52.
6. Yang GCH, Fried KO. Most thyroid cancers detected by sonography lack intranodular vascularity on color doppler imaging: review of the literature and Sonographic-Pathologic correlations for 698 thyroid neoplasms. J Ultrasound Med. 2017;36(1):89–94.
7. Frates MC, Benson CB, Doubilet PM, Cibas ES, Marqusee E. Can color doppler sonography aid in the prediction of malignancy of thyroid nodules? J Ultrasound Med. 2003;22(2):127–31. quiz 132– 124.

8. Lagalla R, Caruso G, Romano M, Midiri M, Novara V, Zappasodi F. [Echo-color doppler in thyroid disease]. Radiol Med. 1993;85(5 Suppl 1):109–13.
9. Adler DD, Carson PL, Rubin JM, Quinn-Reid D. Doppler ultrasound color flow imaging in the study of breast cancer: preliminary findings. Ultrasound Med Biol. 1990;16(6):553–9.
10. Xue N, Li P, Deng H, Yi J, Xie Y, Zhang S. The spoke wheel color doppler blood flow signal is a specific sign of papillary thyroid carcinoma. Front Endocrinol. 2022;13:1030143.
11. Lacout A, Marcy PY, Thariat J. RE: role of duplex doppler US for thyroid nodules: looking for the sword sign. Korean J Radiol. 2011;12(3):400–1.
12. Zhao H, Huang T, Li H. Risk factors for skip metastasis and lateral lymph node metastasis of papillary thyroid cancer. Surgery. 2019;166(1):55–60.
13. Ha EJ, Chung SR, Na DG, Ahn HS, Chung J, Lee JY, et al. Korean thyroid imaging reporting and data system and imaging-Based management of thyroid nodules: Korean society of thyroid radiology consensus statement and recommendations. Korean J Radiol. 2021;22(12):2094–123.
14. Russ G, Trimboli P, Buffet C. The new era of tiradss to stratify the risk of malignancy of thyroid nodules: strengths, weaknesses and pitfalls. Cancers (Basel) 2021, 13(17).
15. Zhou J, Yin L, Wei X, Zhang S, Song Y, Luo B, Li J, Qian L, Cui L, Chen W, et al. 2020 Chinese guidelines for ultrasound malignancy risk stratification of thyroid nodules: the C-TIRADS. Endocrine. 2020;70(2):256–79.
16. Haugen BR, Alexander EK, Bible KC, Doherty GM, Mandel SJ, Nikiforov YE, Pacini F, Randolph GW, Sawka AM, Schlumberger M, et al. 2015 American thyroid association management guidelines for adult patients with thyroid nodules and differentiated thyroid cancer: the American thyroid association guidelines task force on thyroid nodules and differentiated thyroid Cancer. Thyroid. 2016;26(1):1–133.
17. Moon HJ, Kwak JY, Kim MJ, Son EJ, Kim EK. Can vascularity at power doppler US help predict thyroid malignancy? Radiology. 2010;255(1):260–9.
18. Chammas MC, Moon HJ, Kim EK. Why do we have so many controversies in thyroid nodule. Doppler US? Radiol. 2011;259(1):304.
19. Chammas MC, Gerhard R, de Oliveira IR, Widman A, de Barros N, Durazzo M, Ferraz A, Cerri GG. Thyroid nodules: evaluation with power doppler and duplex doppler ultrasound. Otolaryngol Head Neck Surg. 2005;132(6):874–82.
20. Tong MY, Qiu M, Feng X, Guo LY, Xie WL, Jia JJ, Che Y. Coexisting sonographic features of tumor neovascularization-like pattern and echogenic areas in thyroid nodules: diagnostic performance in prediction of papillary carcinoma. Chin Med J (Engl). 2020;133(21):2638–40.
21. Foschini MP, Papotti M, Parmeggiani A, Tallini G, Castaldini L, Meringolo D, Eusebi V. Three-dimensional reconstruction of vessel distribution in benign and malignant lesions of thyroid. Virchows Arch. 2004;445(2):189–98.
22. Padera TP, Stoll BR, Tooredman JB, Capen D, di Tomaso E, Jain RK. Pathology: cancer cells compress intratumour vessels. Nature. 2004;427(6976):695.
23. Rajabi S, Dehghan MH, Dastmalchi R, Jalali Mashayekhi F, Salami S, Hedayati M. The roles and role-players in thyroid cancer angiogenesis. Endocr J. 2019;66(4):277–93.
24. Foschini MP, Ragazzi M, Parmeggiani AL, Righi A, Flamminio F, Meringolo D, Castaldini L. Comparison between echo-color doppler sonography features and angioarchitecture of thyroid nodules. Int J Surg Pathol. 2007;15(2):135–42.
25. Sultan LR, Xiong H, Zafar HM, Schultz SM, Langer JE, Sehgal CM. Vascularity assessment of thyroid nodules by quantitative color doppler ultrasound. Ultrasound Med Biol. 2015;41(5):1287–93.
26. Fukuoka O, Sugitani I, Ebina A, Toda K, Kawabata K, Yamada K. Natural history of asymptomatic papillary thyroid microcarcinoma: Time-Dependent changes in calcification and vascularity during active surveillance. World J Surg. 2016;40(3):529–37.
27. Zhang C, Li B, Zhang L, Chen F, Zhang Y, Cheng W. Clinicopathological and ultrasound features as risk stratification predictors of clinical and pathological nodal status in papillary thyroid carcinoma: a study of 748 patients. BMC Cancer. 2022;22(1):354.
28. Ghossein R, Barletta JA, Bullock M, Johnson SJ, Kakudo K, Lam AK, Moonim MT, Poller DN, Tallini G, Tuttle RM, et al. Data set for reporting carcinoma of the thyroid: recommendations from the international collaboration on Cancer reporting. Hum Pathol. 2021;110:62–72.
29. Huang SS, Yang Z, Li B, Jiang ZH, Tan Y, Hao DD, Chen CQ, Wang YW, Liang JY, Pan FS, et al. Radiating blood flow signal: A new ultrasound feature of thyroid carcinoma. Eur J Radiol. 2024;176:111502.
30. Zhu F, Li Z, Ren J, Wu G, Peng G. Study of relationship between VEGF expression and vasculogenic mimicry of tumor. Chinese-German J Clin Oncol. 2009;8(11):655–8.
31. Folkman J. Is angiogenesis an organizing principle in biology and medicine? J Pediatr Surg. 2007;42(1):1–11.
32. Jia X, Ma Z, Kong D, Li Y, Hu H, Guan L, Yan J, Zhang R, Gu Y, Chen X. Novel human artificial intelligence hybrid framework pinpoints thyroid nodule malignancy and identifies overlooked second-order ultrasonographic features. Cancers. 2022;14(18):4440.
33. Tasci B. Attention deep feature extraction from brain MRIs in explainable mode: DGXAINet. Diagnostics (Basel) 2023; 13(5).

Publisher's note